

# Wind Engineering Joint Usage/Research Center FY2018 Research Result Report

Research Field: Structural Wind Engineering  
 Research Year: FY2018  
 Research Number: 18182002  
 Research Theme: Wind-induced load estimation for clips of standing seam metal roofing system considering dynamic characteristics

Representative Researcher: Y. Q. Li, and Y. Zheng

Budget [FY2018]: 260,000 Yen

## 1. Introduction

In recent years, the standing seam roofing systems, SSRSs, are widely used in modern metal roofs for residential, commercial and even large-scale public buildings due to its advantages of great waterproof, wind-resistant, and temperature stress releasing performance, etc. Generally, the connection detailing are given by the supplier of roofing system according to the design parameters from structural engineers on the contract documents. Therefore, to a structural engineer, how to estimate an effective wind-induced load for clips design considering dynamic characteristics, i.e., unfavorable distribution and fluctuating characteristics of wind, and dynamic effect of roof structure itself, is a key issue for the roof safety. Up to now, the tributary area of a clip,  $A_c$ , and the representative gust pressure,  $P_w$ , is used to estimate the design wind load of a clip,  $F$ , i.e.,  $F = A_c P_w$  (MBMA, 2012<sup>[1]</sup>; GB 51022-2015, 2016<sup>[2]</sup>), and usually a standard checking test is prerequisite to ensure the safety of any new roofing products. However, detachment failure of clips from roof metal panels, as typical and often-happened in practice, invokes further investigation on the accurate and effective wind-induced load estimation of clips connection. An initial work by Jing & Li (2013)<sup>[3]</sup> showed that a magnification coefficient according to typical locations on the roof surface was necessary in comparison with the widely-used tributary area method. Therefore, an effective estimation method for the design wind force of clip is in high demand in practice.

## 2. Experimental set up of wind tunnel tests

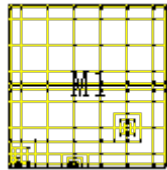
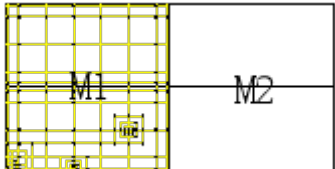
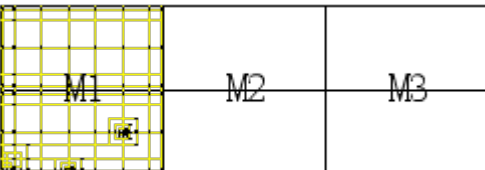
The wind tunnel tests were carried out in the 1.8m (height) × 2.2m (width) × 19m (length) Boundary Layer Wind Tunnel (BLWT) at Wind Engineering Research Center (WERC), Tokyo Polytechnic University (TPU). There are 3 test models all together, including 1 portal frame structure rigid model (M1) with measurement points on the roof surface, and 2 auxiliary models (M2, M3) without any measurement points. M2 and M3 are used as two modules by attaching them to M1 on the lateral surface, in order to obtain the wind pressure data on the roof surface of rigid models with  $L:B = 1:1, 2:1, \text{ and } 3:1$ . The model sizes of M2 and M3 are the same as M1. The relevant parameters of 3 models are listed in Tab. 2.1. There are 174 measurement points totally on the roof surface. According to the regulations of GB 51022-2015<sup>[2]</sup>, the roof is divided into 3 zones, namely the corner zone (Zone A), the edge zone (Zone B) and the center zone (Zone C), respectively. Three typical nodes were selected from Zone A, Zone B, and Zone C, and the number of measurement points around these 3 nodes is increased. The specific measurement point distribution is as shown in Fig. 4.3. The test procedure includes 3 cases, as shown in Tab. 2.2.

Tab. 2.1 Relevant Parameters of 3 Models

Model No.	Geometric Size Ratio	Height (H, mm)	Length (L, mm)	Breadth (B, mm)	Slope	H/B	L/B
M1	1/60	150	300	300	10°	0.50	1.00
M2	1/60	150	300	300	10°	0.50	1.00
M3	1/60	150	300	300	10°	0.50	1.00

Tab. 2.2 Details of Test Cases

Case No.	Model Construction	Modules	Aim

1		M1	To obtain the data in 3 zones of the rigid model with $L:B = 1:1$ .
2		M1 + M2	To obtain the data in 3 zones of the rigid model with $L:B = 2:1$ .
3		M1 + M2 + M3	To obtain the data in 3 zones of the rigid model with $L:B = 3:1$ .

For terrain type, Category II defined in Japanese code (AIJ-04)<sup>[4]</sup> was applied in the tests. The wind speed profile provided in the code and measured during the tests are compared in Fig.2.1, and the turbulence intensity at the eave height of models is about 0.18 (Fig. 2.2). The scale factors, including geometric scale, wind speed scale, time scale, as well as blockage ratio, are listed in Tab. 2.3. As for wind direction, 8 direction cases were considered, including  $0^\circ$ ,  $45^\circ$ ,  $90^\circ$ ,  $135^\circ$ ,  $180^\circ$ ,  $225^\circ$ ,  $270^\circ$  and  $315^\circ$ .

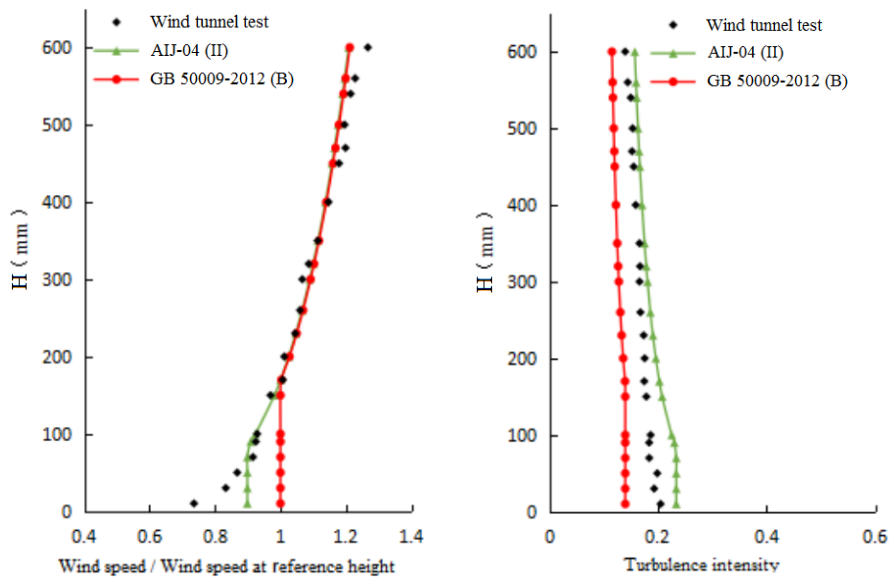


Fig.2.1 Wind Speed Profile in the Tests      Fig. 2.2 Turbulence Intensity in the Tests

Tab. 2.3 Scale Factors in 3 Cases

Factors	Case 1	Case 2	Case 3
Geometric scale	1/60	1/60	1/60
Wind speed scale	1/3	1/3	1/3
Time scale	1/20	1/20	1/20
Blockage ratio (< 5%)	1.48%	2.95%	4.43%

### 3. Pressure distribution measured

Due to the symmetry of the roof, the distribution of average wind pressure coefficient and fluctuating wind pressure coefficient of M1 under the three wind direction angles of  $0^\circ$ ,  $45^\circ$ , and  $90^\circ$  are now counted. The specified pressure is defined as positive when the direction of wind pressure is directed to the roof surface, and vice versa. The average wind pressure coefficient,  $\bar{C}_{pc}$ , and the fluctuating wind pressure coefficient,

$C_{pc}$ , are defined as follow:

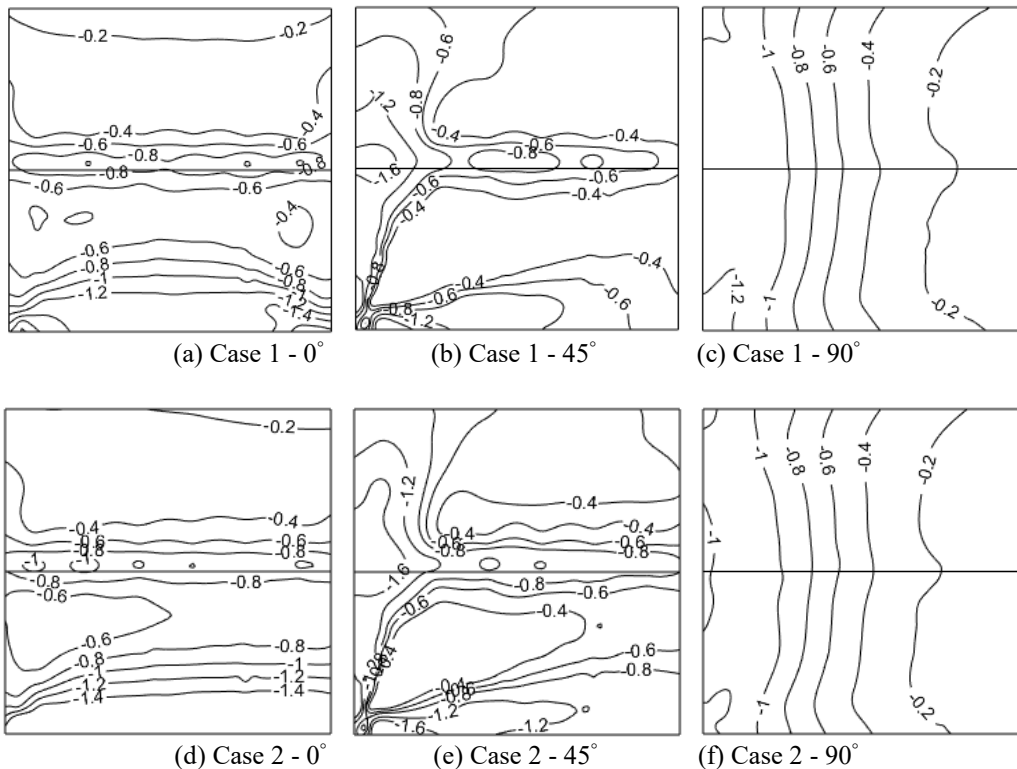
$$\bar{C}_{pc} = \frac{\bar{P}}{q_h}, C_{pc} = \frac{\sigma}{q_h} \quad (3.1)$$

where,  $\bar{P}$ ,  $\sigma$ , and  $q_h$  are the average value of wind pressure, the standard deviation of wind pressure, and the reference wind speed pressure, respectively<sup>[5]</sup>.

The average wind pressure coefficient and the fluctuating wind pressure coefficient of M1 measured in this test are as shown in Fig. 3.1-3.2.

According to Fig. 3.1, the average wind pressure distribution in 3 cases is described as follow: Under wind direction angle  $0^\circ$ , the airflow separates at the junction between the upward wall and the upward roof, and a "separation bubble" is formed within a certain range. Therefore, a large negative pressure is generated at the eaves and the corner of the upward roof, whose absolute value gradually decreases along the direction of the wind. The whole roof surface is under negative pressure. Under wind direction angle  $45^\circ$ , the airflow separates at the corner of the roof, where a small area of separation is formed and a pair of "conical vortex" are formed on the sides of the separation area, so that the area around the "conical vortex" is subjected to a large negative pressure, whose absolute value gradually decreases along the direction of the wind. The whole roof surface is under negative pressure. Under wind direction angle  $90^\circ$ , the average wind pressure coefficient is symmetrically distributed on the roof surface, and the airflow is separated at the junction of the gable and the roof. A "separation bubble" is formed within a certain range, so that a large negative pressure appears on the front edge of the roof, and the absolute value decreases gradually along the direction of the wind. The whole roof surface is under negative pressure.

According to Fig. 3.2, the fluctuating wind pressure distribution in 3 cases is described as follow: Under wind direction angle  $0^\circ$ , large fluctuating wind pressure coefficient appears around the eave and the roof top. Under wind direction angle  $45^\circ$ , the fluctuating wind pressure coefficient is conical and unevenly distributed due to the existence of the "conical vortex", but there is a maximum value near the roof corner. Under wind direction angle  $90^\circ$ , large fluctuating wind pressure coefficient appears around the roof corner. The distribution of the average wind pressure coefficient and the fluctuating wind pressure coefficient in this paper is similar to that of J. D. Holmes's research<sup>[6]</sup>, which proves the rationality of the test data for dynamic time history analysis.



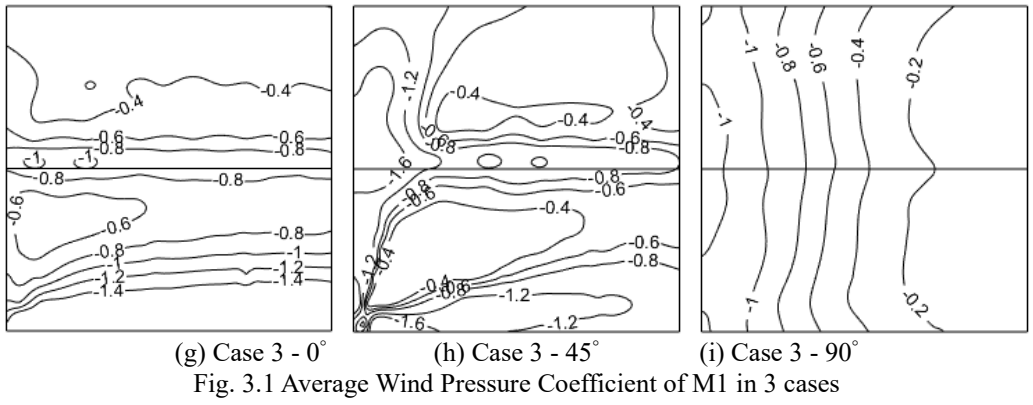


Fig. 3.1 Average Wind Pressure Coefficient of M1 in 3 cases

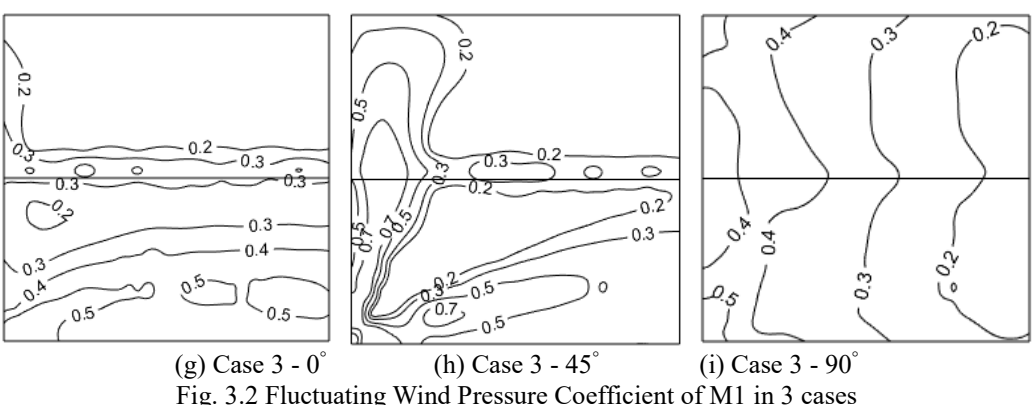
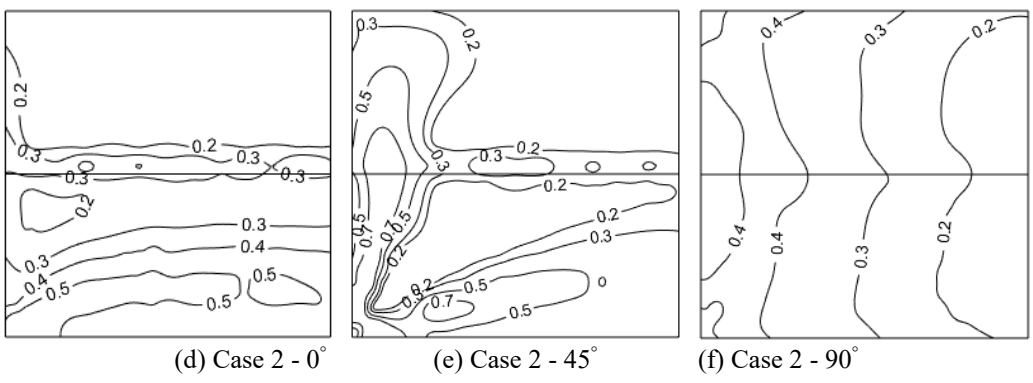
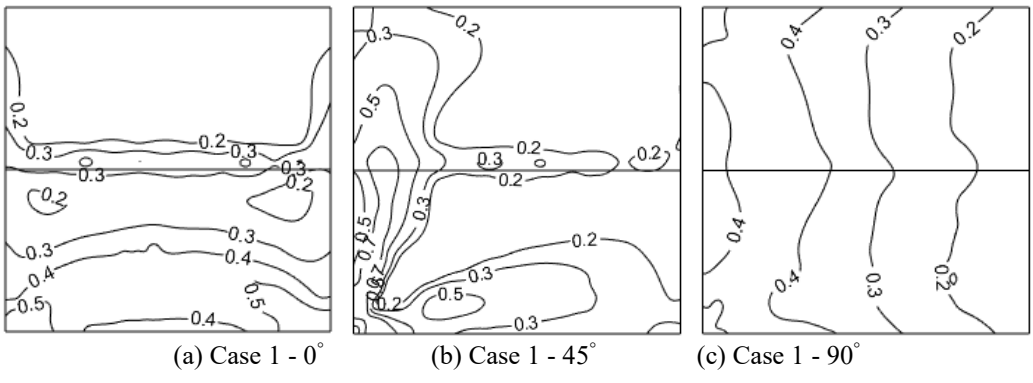


Fig. 3.2 Fluctuating Wind Pressure Coefficient of M1 in 3 cases

#### 4. Finite element analysis

##### 4.1. Finite element model

The ABAQUS finite element model of typical SMRS based on wind load transfer path was established in this paper. The size of the roof is 18m × 9m and the slope angle is 10°. The roof slab is composed of ribbed steel plates, which is equivalent to flat steel plates according to equivalent bending stiffness. The plate width

is 400mm and the thickness is 3.5mm, which is simulated by 3D shell element. The clip mainly plays the role of load transfer element in the roofing system, as a result, it can be simulated by 3D beam element. The purlin is also simulated by 3D beam element, with the spacing of 1.5m and the span of 6m. Z-shaped steel with edge stiffener<sup>[7]</sup> is adopted in the section of purlin. Since the damage of the element itself is not considered in clip design, most of the elements are in elastic state under wind load. Therefore, the ideal elastic model is adopted as the constitutive model. The displacement between neighboring steel plates and the clips is coupled to ensure that the wind load can be transferred from roof plates to the clips. Actually, the self-tapping screws still firmly fix the clips on the purlin under the wind load, so the displacement of the clips and the nodes corresponding to the purlin is directly coupled in the finite element model. In practice, the solid-web purlin is generally designed according to the simple beam. Therefore, the hinge connection is adopted at both ends of the purlin, which can ensure that the wind load can be transferred in the roof components. The ABAQUS finite element model for time history analysis is as shown in Fig. 4.1, and the experiment models in the wind tunnel tests are as shown in Fig. 4.2-4.4.

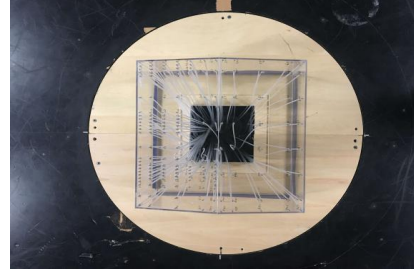
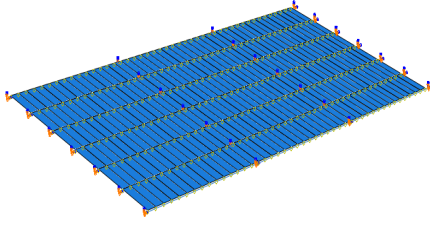


Fig. 4.1 ABAQUS Finite Element Model (Case 1)

Fig. 4.2 Experiment Model (Case 1)

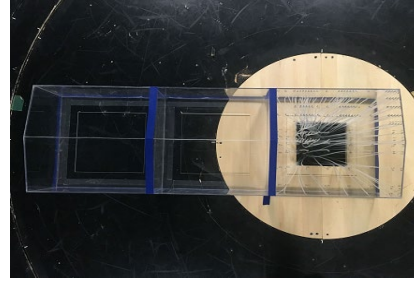
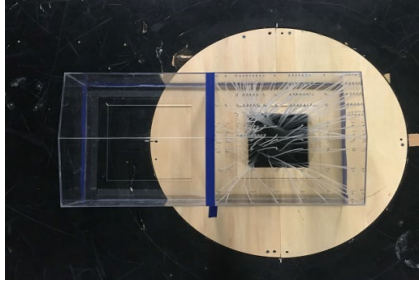


Fig. 4.3 Experiment Model (Case 2)

Fig. 4.4 Experiment Model (Case 3)

The time-domain method is applied in the calculation of the wind-induced response of SMRS, and the relevant parameters are as follows:

- 1) Basic wind pressure, 0.55kPa (the return period is 50 years, considering Shanghai area as an example).
- 2) Time period step, 0.002s (the sampling frequency of the wind tunnel test is 500Hz).
- 3) Structural damping ratio, 0.02<sup>[8]</sup>.
- 4) Rayleigh Damping Model,  $C = \alpha M + \beta K$ , is used in SMRS, which is classic damping system. Coefficients  $\alpha$  and  $\beta$  can be calculated by Equ. 4.1<sup>[9]</sup>.

$$\alpha = \frac{2w_1w_2(\xi_2w_1 - \xi_1w_2)}{w_1^2 - w_2^2}, \quad \beta = \frac{2(\xi_1w_1 - \xi_2w_2)}{w_1^2 - w_2^2} \quad (4.1)$$

#### 4.2. Analysis method

The wind load of the clip is described in the equation below:

$$F_u = P_w A_e \quad (4.2)$$

where,  $P_w$  is the standard value of wind pressure, defined in GB 51022-2015<sup>[2]</sup>.  $P_w$  is taken as 0.55kN/m<sup>2</sup> in this paper, considering Shanghai area.  $A_e$  is the effective wind bearing area of the clip. Amplification factor,  $\eta$ , is defined in Equ. 4.3 to consider the effect of  $A_e$ .

$$F_u = \eta P_w A_c \quad (4.3)$$

where,  $A_c$  is the dependent area of one clip, defined in GB 51022-2015<sup>[2]</sup>.  $\eta$  is the amplification factor of  $A_c$ , which is  $\eta = A_e/A_c$ . The wind pressure time history of the measurement point in wind tunnel test is calculated as follow:

$$F(t) = 0.5\rho v_H^2 C_p(t) A_c \quad (4.4)$$

where,  $\rho$  is the air density,  $v_H$  is the reference wind speed, and  $C_p(t)$  is the wind pressure coefficient time history of the measurement point.

An interpolation method based on the POD method was applied to obtain the wind pressure time history of each node based on the current wind pressure data of limited nodes<sup>[10]</sup>. Firstly, the POD interpolation method was applied based on the limited control points whose number is not locally increased, and the wind pressure data of the clips based on the POD analysis result was separately input to the finite element model for dynamic time history analysis in order to obtain the extreme wind-induced force of the clips. Then, the POD analysis time history data of the clips within a certain range of area  $A_c$ ,  $4A_c$ , and  $9A_c$  was replaced by the actual wind tunnel test data, respectively, and the wind pressure data of the clips based on the updated data was separately input to the finite element model for dynamic time history analysis. Finally, a convergence result will be obtained, which is taken as the final estimated value of  $\eta$  (Fig. 4.3).

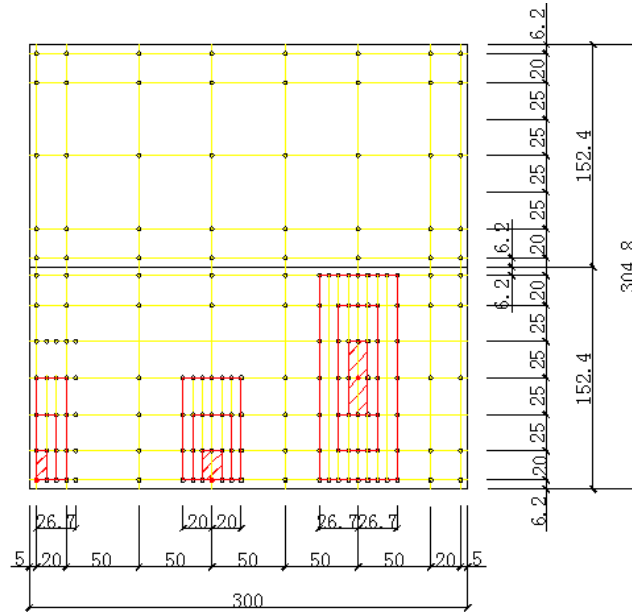


Fig. 4.3 Measurement Point Distribution on the Roof Surface of M1 (mm,  $\alpha = 10^\circ$ )

#### 4.3. Analysis result

Considering the most unfavorable case for clip design, 3 wind direction cases ( $0^\circ$ ,  $45^\circ$ , and  $90^\circ$ ) were analyzed in this paper. Tab. 4.1 gives the finite element calculation result of  $\eta$  for typical clips in 3 zones (Clip 2, 13, and 38 in Zone A, B, and C, respectively) in Case 1 based on GB 51022-2015<sup>[2]</sup>, and the calculated values in bold are the results of the last iteration. It can be concluded that:

- 1) In Zone A and Zone B, the fluctuating wind pressure is large and the wind vortex is remarkable, so as the number of iterations and the analysis area increase gradually, more actual wind pressure data can be utilized compared with the POD interpolation method, the calculation result gradually increases. The
- 2) In Zone C, the fluctuating wind pressure and the average wind pressure are rather small, so as the number of iterations and the analysis area increase gradually, some small data can be replaced by the interpolation value in the POD interpolation method, the calculation result gradually decreases.
- 3) In fact, the effective load bearing area of the clips is limited, so when the analysis area is increased to a certain extent, the value of  $\eta$  is no longer increased, and the iterative result gradually converges. The last iteration result (values in bold) is the final estimation result.
- 4) The first iteration results in zones A, B, and C are about 40%, 80%, and 160% of the second iteration results, respectively, while the second to fourth iteration results are relatively close. This shows that for the nodes in the  $4A_c$  area centered on the clip, using the data based on POD method for dynamic time history analysis has a great influence on the extreme wind-induced force of the clip, while the influence outside the  $4A_c$  area can be neglected.

Tab. 4.1 The Iteration Result of  $\eta$  for Typical Clips in Case 1

Zone No.	Clip No.	Number of Iterations	$0^\circ$	$45^\circ$	$90^\circ$
A	1	1	400.71	270.85	301.01
		2	<b>1028.22</b>	<b>597.79</b>	<b>649.39</b>

		3	1028.62	598.19	649.02
		4	<b>1028.74</b>	<b>598.21</b>	<b>648.67</b>
B	19	1	487.58	332.08	257.57
		2	546.00	423.63	355.17
		3	542.88	422.27	356.93
		4	<b>542.20</b>	<b>422.11</b>	<b>357.47</b>
C	172	1	1067.28	792.07	919.40
		2	615.27	454.33	523.75
		3	597.86	452.16	515.42
		4	<b>596.12</b>	<b>450.32</b>	<b>511.56</b>

There are 20 clips in Zone A, 122 clips in Zone B, and 180 clips in Zone C. Due to space limitations, 8 typical clips from Zone A, 14 typical clips from Zone B, and 15 typical clips from Zone C were selected for analysis. Tab. 4.2-4.4 gives the statistical result of the last iteration for typical clips from 3 zones in Case 1, and the values in bold are the maximum values of  $\eta$  for each wind direction case. The maximum value of  $\eta$  in 3 cases is summarized in Tab. 4.5, and the values in bold are the maximum values of  $\eta$  for each zone. According to Tab. 4.5, it's obvious that due to the spatial correlation of the wind pressure on the roof, the effective wind bearing area of the clips,  $A_e$ , is larger than the dependent area,  $A_c$ . Based on Tab. 4.5, it can be concluded that the length-breath ratio has little effect on the values of  $\eta$  in Zone A and Zone B. The maximum values of  $\eta$  for Case 1 and Case2 are close to each other in Zone C, while the maximum values of  $\eta$  in Case 3 is smaller than that of Case 1 and Case 2, because the wind pressure on the roof is more uniformly distributed as the length-breath ratio increases.

Tab. 4.2 The Calculated Value of  $\eta$  in Case 1

Zone No.	Clip No.	$A_c$ (m <sup>2</sup> )	0°	45°	90°
A	2	0.3	<b>1.37</b>	0.80	0.87
	3	0.3	1.22	1.29	0.88
	4	0.3	1.01	<b>1.65</b>	0.90
	5	0.3	0.95	1.43	0.88
	48	0.6	0.66	1.45	0.87
	49	0.6	0.75	0.67	<b>0.92</b>
	50	0.6	0.82	0.25	0.80
	51	0.6	0.79	0.26	0.82
B	16	0.3	0.90	0.74	<b>0.80</b>
	17	0.3	0.98	0.81	0.72
	18	0.3	1.09	0.85	0.72
	19	0.3	1.14	0.88	0.68
	20	0.3	1.19	0.87	0.64
	21	0.3	1.22	0.88	0.66
	22	0.3	<b>1.25</b>	0.87	0.72
	52	0.6	0.81	0.84	0.62
	53	0.6	0.95	<b>0.93</b>	0.67
	54	0.6	1.04	0.88	0.64
	55	0.6	1.10	0.87	0.58
	56	0.6	1.16	0.84	0.59

	57	0.6	1.20	0.78	0.57
	58	0.6	1.23	0.76	0.57
C	124	0.6	1.59	0.89	0.50
	125	0.6	1.77	0.88	0.65
	126	0.6	1.72	0.81	0.65
	127	0.6	<b>2.02</b>	<b>0.91</b>	0.77
	128	0.6	1.96	0.83	0.79
	170	0.6	1.03	0.71	0.67
	171	0.6	1.05	0.75	0.82
	172	0.6	1.01	0.76	<b>0.86</b>
	173	0.6	1.10	0.82	0.76
	174	0.6	1.08	0.78	0.68
	216	0.6	0.69	0.48	0.52
	217	0.6	0.70	0.68	0.46
	218	0.6	0.73	0.71	0.44
	219	0.6	0.75	0.68	0.45
220	0.6	0.78	0.70	0.49	

Tab. 4.3 The Calculated Value of  $\eta$  in Case 2

Zone No.	Clip No.	$A_c$ (m <sup>2</sup> )	0°	45°	90°
A	2	0.3	<b>1.31</b>	0.96	0.86
	3	0.3	1.19	<b>1.61</b>	0.90
	4	0.3	1.03	1.48	0.91
	5	0.3	1.05	1.26	<b>0.92</b>
	48	0.6	0.67	1.30	<b>0.92</b>
	49	0.6	0.63	0.58	0.79
	50	0.6	0.68	0.61	0.79
	51	0.6	0.73	0.56	0.75
B	16	0.3	0.85	0.90	0.67
	17	0.3	0.85	0.95	<b>0.69</b>
	18	0.3	1.02	0.98	0.68
	19	0.3	1.09	1.03	0.67
	20	0.3	1.15	1.06	0.66
	21	0.3	1.27	1.09	0.66
	22	0.3	<b>1.28</b>	<b>1.10</b>	0.65
	52	0.6	0.87	1.01	0.54
	53	0.6	0.95	1.07	0.59
	54	0.6	1.01	1.01	0.56
	55	0.6	1.07	0.99	0.52
	56	0.6	1.16	0.94	0.53
	57	0.6	1.17	0.98	0.53
58	0.6	1.24	1.01	0.51	
C	124	0.6	1.61	1.27	0.56



	125	0.6	1.65	1.36	0.53
	126	0.6	1.65	1.30	0.48
	127	0.6	<b>2.02</b>	<b>1.49</b>	0.52
	128	0.6	2.00	1.44	0.50
	170	0.6	1.10	1.13	0.50
	171	0.6	1.15	1.23	0.57
	172	0.6	1.24	1.26	0.62
	173	0.6	1.35	1.27	0.61
	174	0.6	1.37	1.31	0.55
	216	0.6	1.08	0.79	0.51
	217	0.6	1.15	0.87	0.55
	218	0.6	1.18	0.86	0.69
	219	0.6	1.20	0.89	0.73
	220	0.6	1.17	1.00	<b>0.76</b>

Tab. 4.4 The Calculated Value of  $\eta$  in Case 3

Zone No.	Clip No.	$A_c$ (m <sup>2</sup> )	0°	45°	90°
A	2	0.3	<b>1.21</b>	1.51	0.88
	3	0.3	1.13	<b>1.62</b>	0.88
	4	0.3	1.01	1.35	0.86
	5	0.3	0.96	1.20	0.89
	48	0.6	0.55	1.25	<b>0.93</b>
	49	0.6	0.61	0.46	0.84
	50	0.6	0.68	0.34	0.71
	51	0.6	0.75	0.49	0.67
B	16	0.3	1.05	0.81	0.69
	17	0.3	1.09	0.92	0.77
	18	0.3	1.17	0.98	<b>0.81</b>
	19	0.3	1.29	1.04	0.80
	20	0.3	1.27	1.07	0.76
	21	0.3	<b>1.33</b>	<b>1.09</b>	0.71
	22	0.3	1.28	1.08	0.66
	52	0.6	0.90	0.96	0.68
	53	0.6	1.01	1.01	0.71
	54	0.6	0.96	1.03	0.70
	55	0.6	0.97	1.07	0.68
	56	0.6	1.02	1.07	0.69
	57	0.6	1.07	1.05	0.66
58	0.6	1.12	1.04	0.52	
C	124	0.6	1.64	1.47	0.56
	125	0.6	1.62	1.52	0.48
	126	0.6	1.56	1.34	0.45
	127	0.6	<b>1.79</b>	1.50	0.51

	128	0.6	1.74	<b>1.57</b>	0.51
	170	0.6	1.23	1.11	0.47
	171	0.6	1.28	1.21	0.53
	172	0.6	1.34	1.26	0.52
	173	0.6	1.44	1.33	0.52
	174	0.6	1.45	1.41	0.52
	216	0.6	0.91	0.84	<b>0.76</b>
	217	0.6	1.12	0.87	0.56
	218	0.6	1.12	0.92	0.52
	219	0.6	1.04	1.03	0.54
	220	0.6	1.13	1.09	0.54

Tab. 4.5 The Maximum Value of  $\eta$  in 3 Cases

Wind Direction	Case 1			Case 2			Case 3		
	Zone A	Zone B	Zone C	Zone A	Zone B	Zone C	Zone A	Zone B	Zone C
0°	1.37	<b>1.25</b>	<b>2.02</b>	1.31	<b>1.28</b>	<b>2.02</b>	1.21	<b>1.33</b>	<b>1.79</b>
45°	<b>1.65</b>	0.93	0.91	<b>1.61</b>	1.10	1.49	<b>1.62</b>	1.09	1.57
90°	0.92	0.80	0.86	0.92	0.69	0.76	0.93	0.81	0.76

## 5. Discussion of analysis result

### 5.1. Comparison with Jing's research

In Jing's research work<sup>[3]</sup>, POD interpolation method was also applied to obtain the dynamic distribution of wind pressure on the whole surface on the basis of the information from the limited measurement points. The efficiency of the analysis result depends on the number of measurement point around the analyzed node in 3 typical zones. However, the number of measurement points around 3 typical zones is quite limited in Jing's model. In this paper, the number of measurement points around the typical clip nodes in corner zone, edge zone, and center area is largely increased (Fig. 4.3) to get a more accurate simulation result when determining the wind-induced load for clips of SSRS. As a result, the further research in this paper is quite necessary to verify the accuracy and practicability of the magnification coefficient,  $\eta$ , focusing on the measurement point distribution method of rigid model. The analysis result of Jing's research is based on CECS 102-2002<sup>[11]</sup>. Therefore, in order to obtain a better comparison result with Jing's research, the magnification factor,  $\eta$ , was recalculated based on CECS 102-2002<sup>[11]</sup>, and the comparison result is as shown in Tab. 5.1.

According to Tab. 5.1, the value of  $\eta$  in this paper is 3.7%~14.8% smaller than that of Jing' research in Zone B and Zone C under various wind direction cases. While in Zone A, the calculation result in this paper is 23.4%~31.4% larger than Jing' result, which is probably because of the number of measurement point in corner area. As mentioned in Section 3, there is an obvious "separation bubble" generated in Zone A under three wind direction angel, 0°, 45°, and 90°, resulting in a significant increase of wind pressure in this area. In this paper, the number of measurement point in Zone A is largely increased, and the description of the increase of local wind pressure is more accurate compared to the result of POD method, so a larger amplification factor was obtained.

Tab. 5.1 Comparison of  $\eta$  with Jing's Research

Case No.	1			2		
Zone No.	A	B	C	A	B	C
This paper	2.43	2.08	2.62	2.37	2.12	2.61
Jing's work	1.85	2.44	2.72	1.92	2.47	3.01
Increase	31.4%	-14.8%	-3.7%	23.4%	-14.2%	-13.3%

### 5.2. Comparison with different codes

The extreme wind force of the clips in 3 cases were calculated based on Chinese code (CECS 102-2002<sup>[11]</sup>,

GB 51022-2015<sup>[2]</sup>, American code (ASCE 7-05)<sup>[12]</sup> and Japanese code (AIJ-04)<sup>[4]</sup>, and the values of  $\eta$  were calculated and compared according to the finite element analysis result. The comparison result is as shown in Fig. 5.1-5.3, and the maximum values of  $\eta$  based on 4 codes are listed in Tab. 5.2. According to Fig. 5.1-5.3 and Tab. 5.2, the following conclusions can be obtained:

- 1) In Zone A and Zone C, the calculated value of  $\eta$  based on AIJ-04 is the smallest among 4 codes, while in Zone B, the calculated value of  $\eta$  based on ASCE 7-05 is the smallest. The calculated value of CECS 102-2002 is the largest in 3 Zones. Generally speaking, the calculated results of GB 51022-2015 and ASCE 7-05 are close to that of AIJ-04, but the maximum value of  $\eta$  in each roof zone exceeds 1.0, indicating that the safety of these 4 codes regarding the extreme wind force of the clips cannot be guaranteed.
- 2) In Zone A (corner zone), the value of  $\eta$  for clips 1-5 is larger than that of clips 6-8, because clips 1-4 are close to the upwind eaves and clip 5 is close to the gable where the wind pressure is relatively large.
- 3) In Zone B (edge zone), the value of  $\eta$  for clips 1-7 is slightly larger than that of clips 8-14, because clips 1-7 are close to the upwind eaves where the wind pressure is relatively large. Generally speaking, the calculated value of  $\eta$  in Zone B fluctuates little.
- 4) In Zone C (center zone), the value of  $\eta$  for is sorted from large to small as: clips 1-5 > clips 6-10 > clips 11-15, because clips 1-5 are located on the row of purlin closest to the upwind eaves while clips 11-15 are close to the rooftop.
- 5) The calculation result differs little between 3 cases, indicating that the length-span ratio ( $L:B$ ) has little effect on the extreme wind force of the clips in each zone.

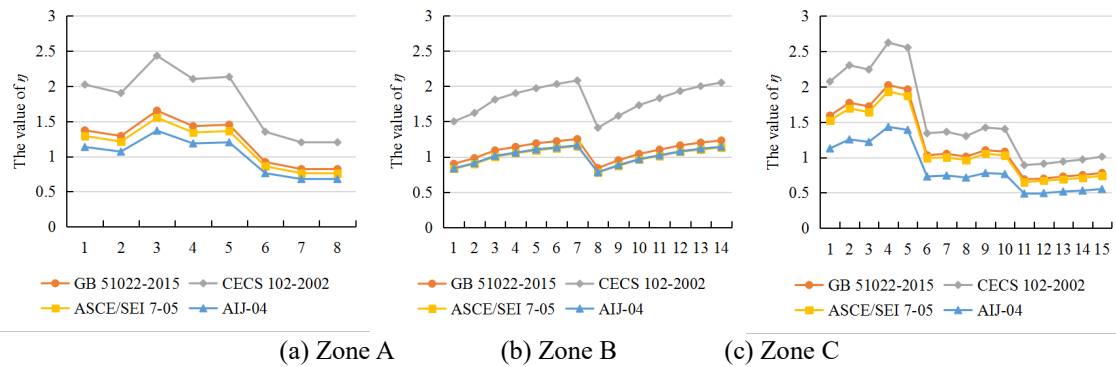


Fig. 5.1 The Calculated Value of  $\eta$  for Typical Clips in Case 1

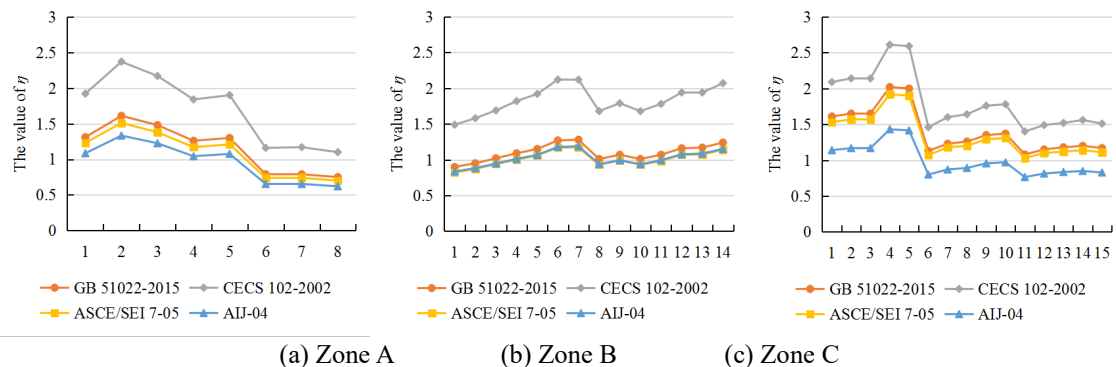
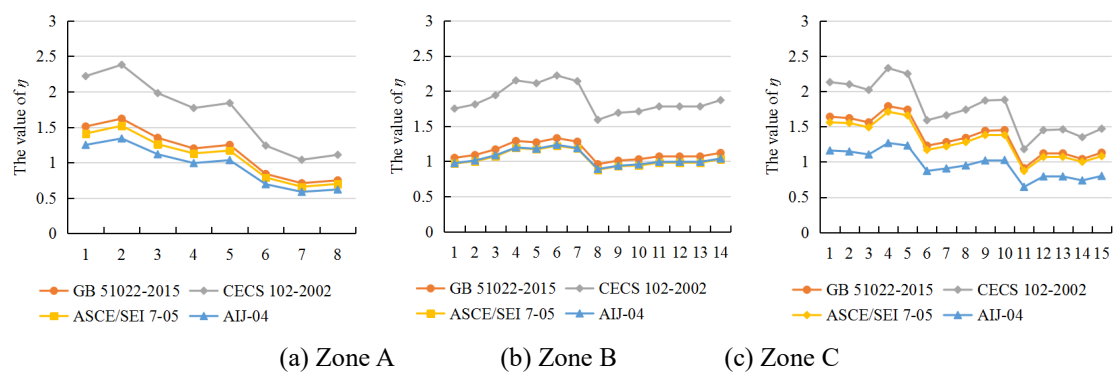


Fig. 5.2 The Calculated Value of  $\eta$  for Typical Clips in Case 2



(a) Zone A (b) Zone B (c) Zone C

Fig. 5.3 The Calculated Value of  $\eta$  for Typical Clips in Case 3

Tab. 5.2 Comparison of  $\eta$  in 4 Codes

Case No.	1			2			3		
	A	B	C	A	B	C	A	B	C
CECS 102-2002	2.43	2.08	2.62	2.37	2.12	2.61	2.38	2.22	2.33
GB 51022-2015	1.65	1.25	2.02	1.61	1.28	2.02	1.62	1.33	1.79
ASCE 7-05	1.55	1.15	1.93	1.51	1.17	1.92	1.52	1.22	1.71
AIJ-04	1.37	1.16	1.43	1.33	1.19	1.43	1.34	1.23	1.27

5.3. Roof zoning in different codes

The relevant regulations about roof zoning of low-rise gable roof with a slope no more than  $10^\circ$  in 4 codes are as shown in Fig. 5.4.

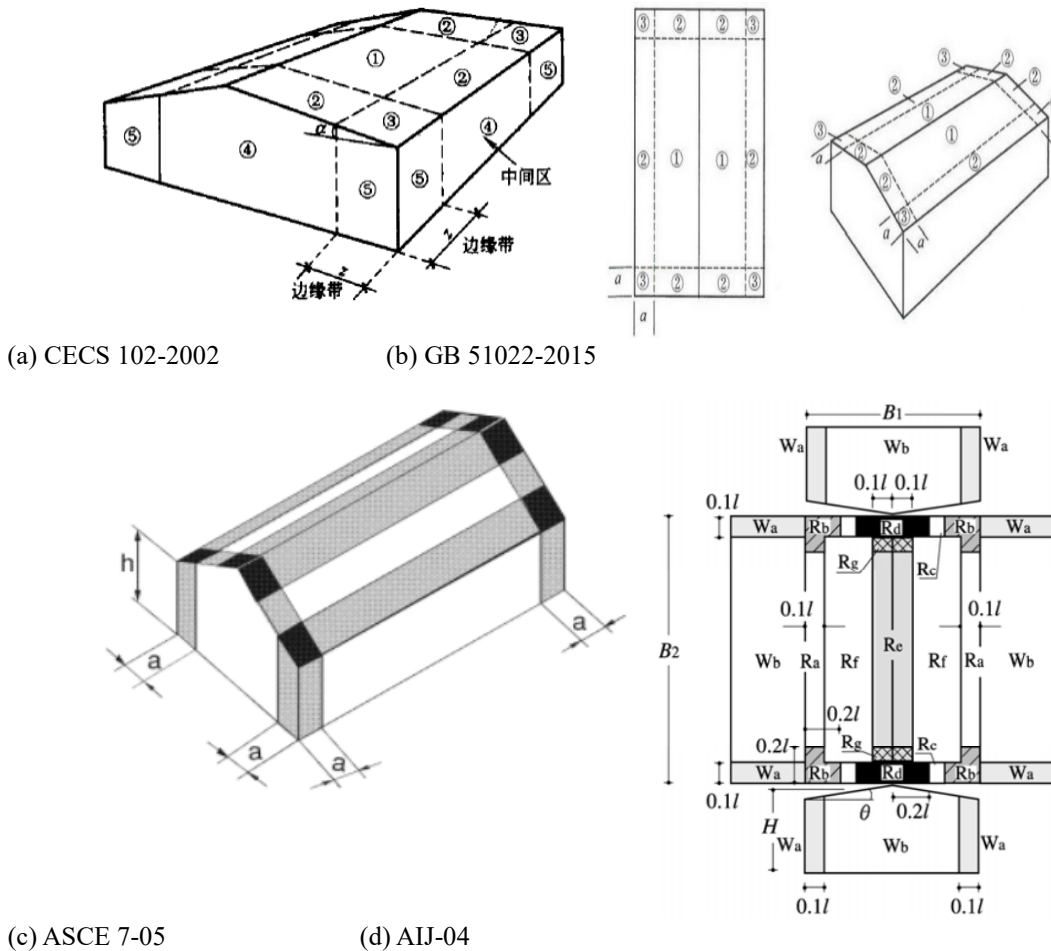


Fig. 5.4 Roof Zoning in 4 Codes

In CECS 102-2002 and GB 51022-2015, the roof is divided into 3 zones, and the edge zone width is the smaller value between 40% of the average roof height and 10% of the minimum horizontal size, but not less than 4% of the minimum house size or 1.0m.

In ASCE 7-05, the roof is also divided into 3 zones, but the ridge areas are considered in the corner and edge zones. The edge zone width is the smaller value between 40% of the eave height and 10% of the minimum horizontal size, but not less than 4% of the minimum house size or 0.9m.

In AIJ-04, the roof is divided into 5 zones considering different roof slope. However, the value of extreme wind coefficient for the roof with a slope no more than  $10^\circ$  is the same in some zones, as a result, there are only 3 roof zones for the roof with a slope no more than  $10^\circ$ . The edge zone width is the smaller value between 40% of the average roof height and 10% of the minimum horizontal size.

#### 5.4. Calculation result in ridge zone based on ASCE 7-05

As ASCE 7-05 divides the roof ridge zone into corner zone and edge zone (ASCE method), while AIJ-04 and GB 51022-2015 define the roof ridge zone as edge zone and center zone (AIJ method). In order to verify the reliability of roof zoning, the wind-induced force of clips in the roof ridge zone based on ASCE 7-05 is analyzed in this section. Take case 1 for example, 8 clips from ridge-corner zone and 14 clips from ridge-edge zone are chosen for analysis. The analysis result is as shown in Fig. 5.5.

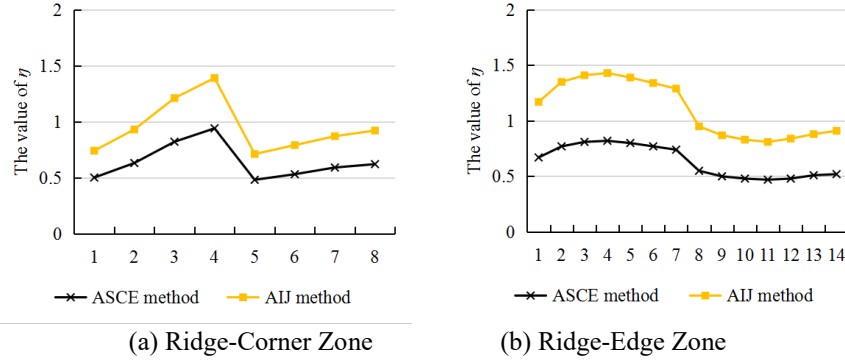


Fig. 5.5 The Calculated Value of  $\eta$  in Ridge Zone Based on ASCE 7-05

Comparing Fig. 5.1 and Fig. 5.5, the extreme wind force level in ridge-corner zone is equivalent to that in the corner zone of the roof, and the extreme wind force level in ridge-edge zone is equivalent to that in the center zone of the roof. Therefore, using the "ASCE method" for roof zoning is conservative and overestimates the extreme wind-induced force of the clips in roof ridge area. In summary, the corner area and the edge area of the ridge can be classified as corner zone and center zone of the roof.

#### 5.5. Recommended value of $\eta$ based on different codes

According to the summary result in Tab. 5.2, the recommended values of  $\eta$  based on CECS102-2002, GB 51022-2015, ASCE 7-05 and AIJ-04 are concluded in Tab. 5.3.

Tab. 5.3 Recommended Values of  $\eta$  in Various Codes

Roof Zoning	A	B	C
CECS 102-2002	2.5	2.3	2.7
GB 51022-2015	1.7	1.4	2.1
ASCE 7-05	1.6	1.3	2.0
AIJ-04	1.4	1.3	1.5

Note: The roof zoning is adopted in accordance with the provisions of each code. The corner area and the edge area of the ridge are considered as corner zone and center zone in each code, respectively.

## 6. Conclusion

In this paper, considering the actual influence range of the bearing force for clips of SMRS and the spatial correlation of the fluctuating wind on the roof, an effective estimation method for extreme wind-induced force for clips of SMRS is proposed. Based on the wind tunnel test data, the finite element model was established to obtain the dynamic time history analysis results. The dependent area,  $A_c$ , defined in GB 51022-2015 was compared with the time history analysis results. As a result, the concept of effective wind bearing area was introduced into the estimation of the effective static wind-induced force of the clips, thereby drawing the concept of magnification coefficient,  $\eta$ . The following conclusions were reached:

- 1) For double-slope roofs with a slope of  $10^\circ$  under various wind direction angles, the whole roof is under negative wind pressure. In the case of wind direction  $0^\circ$ , the eaves and the corner are subjected to a large negative pressure; in the case of wind direction  $45^\circ$ , the wind cone area around roof corner is subjected to a large negative pressure; in the case of wind direction  $90^\circ$ , the eaves of the upward roof is subjected to a large negative pressure.
- 2) The length-span ratio of the house has little effect on the average wind pressure coefficient of the roof when it's is greater than 3. The length-span ratio of has little effect on the fluctuating wind pressure coefficient in local areas such as the corner area and the edge area.
- 3) When calculating the extreme wind-induced force of the clips using finite element analysis, the

POD interpolation method homogenizes the wind pressure of some areas (such as the corner zone and the edge zone) to some extent. Therefore, increasing the number of measurement points performing in these areas and replacing the POD analysis result with the actual wind pressure time history can result in more accurate analysis results.

4) For double-slope roofs with a slope of  $10^\circ$ , the roof zoning in various codes is introduced, and the values of the magnification coefficient,  $\eta$ , based on various codes are recommended in Tab. 5.3. As for the value of  $\eta$ , CECS 102:2002 has the largest calculated value, which is about 70%-90% higher than other 3 codes. In corner zone and edge zone, The calculated value of  $\eta$  based on GB 51022-2015 is slightly larger, but it is closer to the calculated results of ASCE-705 and AIJ-04. In center zone, the calculated result of AIJ-04 is rather small, which is about 70% of the calculated results based on GB 51022-2015 and ASCE 7-05. Overall, the calculated values of  $\eta$  based on 4 codes are basically greater than 1.0.

### Acknowledgement

The authors are grateful to the financial support of the Joint Usage/Research Center (JURC) project “Wind-induced Load Estimation for Clips of Standing-seam Roofing System Considering Dynamic Characteristics” from Tokyo Polytechnic University, (2018 FY), and the National Natural Science Foundation of China (No. 51478331).

### References

- [1] Metal Building Manufacturers Association (MBMA): *Metal Roofing Systems Performance Guide Specification*, USA, 2012.
- [2] *Technical Specification for Steel Structure of Light-Weight Buildings with Gabled Frames* (GB 51022-2015), China, 2016.
- [3] X. K. Jing, Y. Q. Li: Effective Static Wind Load for Clips of Standing Seam Roofing System, *Journal of Tongji University*, Vol.41, pp.1630-1635, 1760, 2013.
- [4] Architectural Institute of Japan (AIJ): *Recommendations for Loads on Building*, Japan, 2004.
- [5] Wind Tunnel Research Guidelines Committee: *Wind Tunnel Experiment Guide*, Japan, 2011.
- [6] J. D. Holmes: Wind Pressures on Tropical Housing, *Journal of Wind Engineering and Industrial Aerodynamics*, Vol.53, pp.105-123, 1994.
- [7] *Technical Specification of Cold-formed Thin-wall Steel Structure* (GB 50018-2002), China, 2003.
- [8] *Code for seismic design of buildings* (GB 50011-2010), China, 2010.
- [9] Z. D. Yu: Structural dynamics basis, *Tongji University Press*, 1987.
- [10] Y. Tamura, H. Ueda, et al.: Proper Orthogonal Decomposition Study of Approach Wind-building Pressure Correlation, *Journal of Wind Engineering and Industrial Aerodynamics*, Vol.72, pp.421-431, 1997.
- [11] *Technical Regulation for Steel Structure of Light-Weight Buildings with Gabled Frames* (CECS 102-2002), China, 2003.
- [12] ASCE Standard No. 7-05: *Minimum Design Loads for Buildings and Other Structures*, USA, 2005.
- [13] J. D. Ginger, J. D. Holmes: Effect of Building Length on Wind Loads on Low-rise Buildings with a Steep Roof Pitch, *Journal of Wind Engineering and Industrial Aerodynamics*, Vol.91, pp.1377-1400, 2003.

### Research Group

1. Representative Researcher  
Y. Q. Li  
Y. Zheng  
X. K. Jing
2. Collaborate Researchers  
A. Yoshida

### Abstract (half page)

#### Abstract

This project mainly focuses on the establishment of an effective static estimation method for extreme wind-induced load for clips of the standing seam metal roofing system (hereinafter referred to as SSRS) considering dynamic characteristics of wind and structure. Firstly, simultaneous pressure measurement on rigid gable roof models was conducted mainly considering length-span ratio in the BLWT of Tokyo Polytechnic University, Japan, for the establishment of a test database for subsequent research. Then, finite

element modelling for SSRS according to wind load path in the roofing system was done to check the effective wind loaded area for clips in typical zones on the roof surface based on the traditional tributary wind loaded area, and the spatial correlation of fluctuating wind pressure on the roof surface, as well as the dynamic effect of roof structure itself. According to Chinese code, American code and Japanese code, a magnification coefficient based on the traditional tributary wind loaded area was calculated and compared. Finally, an estimation method of effective wind-induced load for the clips with proposed amplifying factors in typical zones considering dynamic characteristics was established to simplify the wind-induced load estimation for clips design of SSRS.